

Document downloaded from:

<http://hdl.handle.net/10251/78066>

This paper must be cited as:

Fernández Domene, RM.; Sánchez Tovar, R.; Escrivá Cerdán, C.; Leiva García, R.; Garcia-Anton, J. (2015). Comparison of the effect of non-polluted and underwater-volcano-polluted seawater on the corrosion resistance of different stainless steels. *Materials and Corrosion / Werkstoffe und Korrosion*. 66(11):1279-1289. doi:10.1002/maco.201408172.



The final publication is available at

<http://dx.doi.org/10.1002/maco.201408172>

Copyright Wiley

Additional Information

# COMPARISON OF THE EFFECT OF NON-POLLUTED AND UNDERWATER-VOLCANO-POLLUTED SEAWATER ON THE CORROSION RESISTANCE OF DIFFERENT STAINLESS STEELS.

R.M Fernández-Domene<sup>a</sup>, R. Sánchez-Tovar<sup>a</sup>, C. Escrivà-Cerdán<sup>b</sup>, R. Leiva-García<sup>b</sup>, J. García-Antón<sup>a\*</sup>

<sup>a</sup>Ingeniería Electroquímica y Corrosión. Dpto. Ingeniería Química y Nuclear. Universitat Politècnica de València. C/ Camino de Vera s/n. 46022 Valencia, Spain.

\*jgarciaa@iqn.upv.es

<sup>b</sup>School of Materials, University of Manchester, Manchester M13 9PL, UK

## Abstract

This work compares the effect of non-polluted and underwater-volcano-polluted seawater on the electrochemical behavior of two different alloys, notably an austenitic stainless steel (SS) and a duplex stainless steel. Polarization measurements, potentiostatic passivation tests, electrochemical impedance spectroscopy and capacitance measurements were performed. Results show that the composition of the polluted seawater negatively affects the passivation kinetics of both AISI 316 SS and Alloy 900, decreasing the corrosion resistance of both alloys. Additionally, when both steels are compared, it can be concluded that passive films formed on Alloy 900 presented better protective properties than those on AISI 316 SS.

*Keywords: Volcanic eruption; Stainless steel; passive films; EIS; Mott-Schottky analysis.*

## 1. Introduction

Last 10<sup>th</sup> of October of 2011 a volcano erupted in the Atlantic Ocean near the island of El Hierro (Canary Islands, Spain). During a subsea volcano eruption gases and thermal water emissions, CO<sub>2</sub> being the main gas (around 90 %) are released. This could cause a decrease of the seawater pH value and modify the behavior of the materials which are in contact with this medium <sup>[1-4]</sup>.

Materials for marine applications are selected to maintain the integrity of the structure (i.e. to be sufficiently robust withstand their service environment) and to be corrosion resistant. Stainless steels are used in marine applications because they are resistant to corrosion, easily fabricated and offer good mechanical properties. However, Stainless steels (SS) are susceptible to localized corrosive attacks, such as pitting corrosion, intergranular corrosion and stress corrosion cracking in highly electrical conducting media, such as seawater. Corrosion can cause great damages to marine steel infrastructures such as bridges, wharfs, platforms and pipeline systems <sup>[5]</sup>. These corrosion problems could be aggravated if the medium is altered, due to volcano emissions, since the resistance of the surface film is influenced by the pH <sup>[6]</sup>. Therefore, an adequate selection of the materials is quite important; austenitic stainless steel grades 1.4401 (AISI 316) and its derivatives are suitable for coastal service environments, splash zone applications and intermittent submersion in seawater. Duplex stainless steels (e.g. 1.4462/ASTM S31803) may be used in brackish waters (e.g. estuaries where the chloride content of the water is less than that of the open sea). Superduplex stainless steels (e.g. 1.4410/ASTM S32750) may also be used in direct and prolonged contact with seawater (e.g. in offshore oil platforms).

In a previous work <sup>[7]</sup>, a comprehensive study of the passivation/corrosion behavior of AISI 316L stainless steel was performed; the novelty of the study lied in the electrolyte used (polluted seawater collected from the volcano of El Hierro Island) and the results showed a clear influence of the polluted water on the passivation properties of the AISI 316L. Now, the main objective of this work is to compare the influence of the non-polluted and polluted seawater on the electrochemical properties of two different stainless steels, notably the austenitic stainless steel AISI 316 and the duplex stainless

steel UNS 1.4462 (Alloy 900) by using different electrochemical techniques, i.e. potentiodynamic curves, electrochemical impedance spectroscopy (EIS) and the Mott–Schottky analysis.

## 2. Experimental procedure

### 2.1. *Materials, solution and electrochemical cell*

Experiments were performed in non-polluted and polluted seawater. The coordinates where the seawater samples were taken are shown elsewhere<sup>[7]</sup>, as well as the main parameters of the seawaters<sup>[7]</sup>.

The materials tested were AISI 316 stainless steel and duplex stainless steel, Alloy 900, the composition in weight percent of both steels is shown in **Table 1**. The electrodes were cylindrically shaped (8-mm in diameter and 55 mm long) and covered with a polytetrafluoroethylene (PTFE) coating. The total area exposed to the solution was 0.5 cm<sup>2</sup>. All specimens were wet abraded from 500 to 4000 SiC grit, and finally cleaned with ethanol, rinsed with distilled water and air-dried.

To perform the electrochemical tests a sheathed vertical electrochemical cell was used. The cell was made of glass and allows the introduction of three electrodes: a silver-silver chloride (Ag/AgCl 3M KCl) reference electrode, a platinum (Pt) wire as an auxiliary electrode and the working electrode. Electrochemical measurements were performed to the stainless steels using an Autolab PGSTAT302N potentiostat, in both non-polluted and polluted seawater, at 25° C. In all cases the tests were repeated at least three times in order to verify reproducibility.

## 2.2. Polarization tests

Polarization tests began at a potential value of  $-250 \text{ mV}_{\text{Ag}/\text{AgCl}}$  with respect to the open circuit potential and the potential was subsequently scanned anodically until the current density reached  $10 \text{ mA}/\text{cm}^2$ , where the potential scan was reversed. A scan rate of  $0.5 \text{ mV}\cdot\text{s}^{-1}$  was used.

## 2.3. Potentiostatic passivation tests

Before the passivation experiments, the electrode potential was kept at a cathodic value of  $-0.4 \text{ V}_{\text{Ag}/\text{AgCl}}$  for 15 minutes, to create reproducible initial conditions. Afterwards, the working electrode was polarized at  $-0.1 \text{ V}_{\text{Ag}/\text{AgCl}}$  for 1 hour, in both non-polluted and polluted seawater at  $25^\circ \text{ C}$ , to form a steady-state passive film. During passivation experiments, current density was recorded against time. Current density transients have been used to obtain the passivation time,  $t_p$ .

## 2.4. EIS and capacitance measurements

EIS and capacitance measurements were performed after passivation tests, once a stable passive film was formed on the surface of the samples. EIS measurements were conducted separately at Open Circuit Potential (OCP) and at the applied potential of  $-0.1 \text{ V}_{\text{Ag}/\text{AgCl}}$  in the frequency range of  $100 \text{ kHz}$ - $10 \text{ mHz}$ , with a signal amplitude of  $10 \text{ mV}$ . Additionally, the capacitance of the interface was calculated at a constant frequency of  $5 \text{ kHz}$  using a  $10 \text{ mV}$  amplitude signal and scanning the potential from  $-0.1 \text{ V}_{\text{Ag}/\text{AgCl}}$  in the negative direction at a rate of  $25 \text{ mV s}^{-1}$ . A high scanning rate was used to avoid electroreduction of the passive film and changes in film thickness during the measurements. At a sufficiently high scanning rate, the defect structure within the

passive film is “frozen-in”, to avoid the defect density from being affected by the change of the applied potential.

### 3. Results and discussion

#### 3.1. OCP

**Table 2** shows the mean values corresponding to the last-five-minutes of one hour of the open circuit potential tests obtained for the alloys in the non-polluted and polluted sea waters. According to **Table 2**, there is no influence of the media (non-polluted or polluted) on the OCP, since the values are of the same magnitude order, both for AISI 316 and Alloy 900. On the other hand, the OCP values obtained for the Alloy 900 in the non-polluted and polluted seawaters are slightly more negative than those determined for the AISI 316 SS.

#### 3.2. Polarization tests

**Figure 1** shows the cyclic polarization curves obtained in both seawater media. As tests were reproducible, the curves shown illustrate one of the recorded measurements. Corrosion potential ( $E_{corr}$ ), passivation current density ( $i_p$ ), pitting potential ( $E_p$ ) and repassivation potential ( $E_{rp}$ ) were obtained from cyclic polarization curves (**Table 3**). According to **Table 3**,  $E_{corr}$  values are of the same magnitude order regardless the media, moreover, the values are similar for both alloys. Additionally, **Table 3** shows the  $i_p$  values which determine the corrosion rates of the passive alloy. Their values were obtained as the mean values where current density remains stable when potential shifts to the anodic direction. According to the obtained values,  $i_p$  significantly increases in polluted sea waters, this fact could be related with the lower pH find in polluted seawater. On the other hand, the  $i_p$  values of Alloy 900 are slightly higher than the

obtained for AISI 316 SS. Corrosion rates of AISI 316 and Alloy 900 are likely to be of the same order of magnitude since the corrosion resistance of these alloys is provided by the Cr(III)-rich passive film<sup>[8]</sup>. **Figure 1** shows that current fluctuations appeared in the passivation region of the alloys, except for the Alloy 900 in non-polluted seawater. Therefore, AISI 316 and Alloy 900 in polluted seawater are more prone to metastable pitting<sup>[9]</sup>.  $E_p$  indicates pitting corrosion susceptibility to local breakdown and stable pit initiation and they were determined as the potential at which current density reaches  $100 \mu\text{A}/\text{cm}^2$ <sup>[10]</sup>. Chlorides, which are present in seawater, are aggressive ions that promote passive film breakdown of stainless steel<sup>[10, 11]</sup>, consequently, both alloys are susceptible to pitting corrosion in non-polluted and polluted sea waters.  $E_p$  values are of the same magnitude order regardless the media, the values being slightly more positive in the non-polluted seawater. However, it is noteworthy the more positive  $E_p$  values obtained for the Alloy 900. In general, the duplex alloys offer a number of advantages over the austenitic stainless steels, including: increased resistance of duplex alloys to localised corrosion due to the higher N, Cr and Mo contents than corresponding austenitic stainless steels (**Table 1**).

### *3.3. EIS measurements at open circuit potential*

Electrochemical impedance spectroscopy was employed to investigate the electrochemical behaviour of the films formed on the different steels at open circuit potential. The impedance responses are presented in Nyquist and Bode formats in **Figure 2** and **Figure 3** for AISI 316 SS and Alloy 900, respectively in the polluted and non-polluted seawater. All impedance spectra present a somewhat unfinished capacitive arc which as evidenced from **Figures 2** and **3**, which show that the overall impedance

values slightly decrease in the polluted seawater. The high impedance values along with the phase angle values, which are very close to 90°, suggest that stable films are formed on the surface of the electrodes <sup>[12-15]</sup>. In order to take into account this deviation from the ideal capacitor behaviour, the use of a constant phase element (*CPE*) was necessary, due to the distribution of relaxation times as a consequence of heterogeneities on the electrode surface <sup>[16]</sup>. The impedance of this element is defined as <sup>[17]</sup>:

$$Z_{CPE} = \frac{1}{Q (j\omega)^n} \quad (1)$$

where  $Q$  is the *CPE* constant,  $\omega$  is the angular frequency (rad/s),  $j^2 = -1$  is the imaginary number and  $n$  is the *CPE* exponent. Depending on  $n$ , *CPE* can represent resistance ( $n = 0$ ,  $Z_0 = R$ ), capacitance ( $n = 1$ ,  $Z_0 = C$ ), or Warburg impedance ( $n = 0.5$ ,  $Z_0 = W$ ).

The *CPE* elements,  $Q$ , have been converted into a pure capacitance ( $C$ ) by means of the following equation <sup>[16]</sup>:

$$C = \frac{(Q \cdot R)^{1/n}}{R} \quad (2)$$

Two time constants appeared overlapped in the Bode plots which has been considered as the response of an inhomogeneous film composed of a bilayer structure of the passive films, i.e. a compact inner layer and a less compact outer layer <sup>[8, 18-20]</sup>. According to this behaviour the hierarchically distributed equivalent circuit, reproduced in **Figure 4** has been proposed <sup>[13, 21, 22]</sup> to model the experimental data represented in **Figure 2** and **Figure 3** at OCP. The quality of data fitting to the equivalent circuit

proposed was evaluated with the chi-squared ( $\chi^2$ ) values, which were of the order of  $10^{-3}$ . The physical description of the model adopted is that  $R_1$ ,  $C_1$  and  $R_2$ ,  $C_2$  correspond to the resistance and capacitance of the outer porous layer and inner oxide layer, respectively. In this sense, the time constant observed at high frequencies is represented by the resistance of the solution in the defects of the porous film ( $R_1$ ) and the double layer capacitance in the defects ( $C_1$ ). The second time constant at lower frequencies is assigned to the areas covered with the passive oxide film (protective oxide) and is represented by the  $R_2/C_2$  parallel combination, representing the electrical resistance and the capacitance of the passive oxide film formed as an inner layer on steels. The resistance at very high frequencies corresponds to the uncompensated resistance of the solution ( $R_s$ ).

The electrical parameters obtained by adjusting the experimental data shown in **Figures 2 and 3** are summarised in **Table 4**. According to the electrical parameters obtained, the resistance of the inner oxide layer ( $R_2$ ) is larger than the values associated with the outer layer ( $R_1$ ), which is consistent with the chosen physical model. These results indicate that the protection provided by the passive film is mainly due to the inner passive layer, known as the barrier layer, which is composed principally of chromium oxides. The resistance of the outer porous layer  $R_1$  depends strongly on the existence of pores or defects, into which the electrolyte can penetrate and thus,  $R_1$  provides a sensitive indication of the appearance of defects in the passive film.  $C_1$  values are of the order of those expected for a double layer capacitance<sup>[17]</sup>, showing higher values in the polluted seawater for both steels. Some authors<sup>[21, 23]</sup> have correlated capacitance values with the thickness of the passive layers through the expression (3)<sup>[17]</sup>:

$$C = \frac{\epsilon \cdot \epsilon_0}{d} \quad (3)$$

where  $\epsilon$  denotes the relative dielectric constant of the layer,  $\epsilon_0$  is vacuum permittivity ( $8.85 \times 10^{-14}$  F cm<sup>-1</sup>) and  $d$  is the layer thickness. Although it is difficult to obtain an accurate value for the dielectric constant, this expression can give an indication of how the thickness of the passive films changes in the different conditions, since capacitance is inversely proportional to layer thickness. In this sense,  $C_1$  values reveal that the thickness of the outer layer decreases in the polluted seawater for both alloys.

On the other hand, the parameters associated with the inner oxide layer,  $R_2$ ,  $C_2$ , reveal that the electrical conductivity of the film increases in the polluted seawater, which is indicated by the decrease in the resistance  $R_2$  for both alloys. The increase in the capacitance  $C_2$  may indicate that the inner oxide film becomes thinner and this is especially observed in the 316SS when it is immersed in the polluted seawater.

To compare the corrosion resistance provided for each steel, the polarisation resistance,  $R_p$  has been calculated as the sum of  $R_1 + R_2$  (**Table 4**). The passive films become less protective in the polluted seawater for both steels, which is revealed by the decrease in the polarisation resistance. However, it is noteworthy that the resistance of the Alloy 900 in the polluted seawater is slightly higher than that observed for the AISI 316SS, which means that Alloy 900 developed a more protective passive film in this medium.

#### 3.4. *Potentiostatic passivation tests*

The current-time transients of AISI 316SS and Alloy 900 obtained in both non-polluted and polluted seawater are shown in **Figure 5**. The values of the current density recorded during the potentiostatic passivation tests give the total current resulting from the

formation and dissolution of the films on the alloys in the different solutions studied [24, 25]. When passive films are formed, the dissolution current is usually very small, unless metal dissolution is dominated by pitting or general corrosion [26-28], therefore, it is assumed that the measured current density due to metal dissolution is insignificant compared to that of the passive film formation.

The shape of the transients in **Figure 5** indicates that these are passive systems, since the current density exponentially decreases with time while the passive film is growing on the surface of the alloy and reaching a very low steady-state value of the current density ( $i_{ss}$ ) after 1h of passivation. It is noteworthy that during the first 300s of the test, current density values are higher in the polluted seawater for both alloys, although this difference is more marked in the AISI 316SS.

The passivation rate of a metal or alloy can be compared in terms of the time required to achieve a predetermined degree of passivation after stepping the potential from the cathodic cleaning potential to the formation potential, which is known as passivation time ( $t_p$ ) [26-29]. The shorter the passivation time, the faster the passivation rate of an alloy. Taking an arbitrary value of passive current density of  $i_r = 0.5 \mu\text{A}/\text{cm}^2$ , similar to the values of passive current density obtained from the polarization curves (**Figure 1**), passivation time can be determined from the current-time transients show in **Figure 5**. The values for  $t_p$ , as well as, for the steady-state current density reached for each system are summarized in **Table 5**. Passivation times are shown to be higher in the polluted seawater for both alloys.  $t_p$  increases in the polluted seawater with respect of the non-polluted seawater. These results confirm that the passivation process in the polluted

seawater is slowed down for both alloys, although it is more pronounced in the AISI 316SS.

Finally, the current density at the steady-state after 1h of passivation ( $i_{ss}$ ) shows slightly higher values for the polluted seawater for both alloys. After this period of passivation process, AISI 316SS is able to reach lower values regardless the seawater used in comparison with the Alloy 900.

### *3.5. EIS measurements at an applied anodic potential*

Passive films have also been anodically formed at  $-0.1 V_{Ag/AgCl}$  on AISI 316 SS and Alloy 900 in the non-polluted and polluted seawater, at  $25^{\circ} C$ , in order to study their semiconducting properties. The film formation potential has been selected using the polarization curves of both stainless steels (**Figure 1**). **Figures 6** and **7** show the EIS spectra of AISI 316 SS and Alloy 900 in the form of Nyquist and Bode plots. In all the cases, EIS plots display the typical features of a passive system, that is, very high impedance values and a non-ideal capacitive behavior (phase angles never reach a value of  $-90^{\circ}$ ). These results suggest the formation of a highly stable passive film on the electrodes surface <sup>[12-15]</sup>. In general, higher impedance values are observed for those passive films formed in non-polluted seawater.

The equivalent circuit used above to interpret the EIS data recorded at the open circuit potential, consisting of two hierarchical parallel RC time constants (**Figure 4**), has also been used to fit the experimental EIS results obtained under anodic polarization. Although the fits were acceptable from a mathematical point of view ( $\chi^2$  of the order of

$3 \cdot 10^{-3}$ ), the values of the  $CPE_2$  exponent ( $n_2$ ) were close to 0.5 in all the cases.  $n_2 \approx 0.5$  is a typical value for mass transfer processes at low frequencies, which can be better represented by a Warburg element <sup>[30, 31]</sup>. Therefore, an alternative equivalent circuit including a Warburg element replacing the second RC time constant has been used to interpret experimental EIS data (**Figure 8**). Therefore, depending on the film formation conditions (spontaneous formation in contact with the electrolyte at the open circuit potential or imposing an anodic constant potential), different equivalent circuits may be necessary <sup>[31]</sup>.

In this second equivalent circuit (**Figure 8**),  $R_S$  is the electrolyte resistance, the time constant  $R_I CPE_I$  accounts for the properties of the passive film/electrolyte interface ( $R_I$  is charge transfer resistance and  $CPE_I$  is related to the capacitance of the film/electrolyte interface, which behaves as a non-ideal capacitor), while the Warburg impedance has been used to explain the transport of point defects within the passive film <sup>[15, 30-37]</sup>. The Warburg impedance is defined by the following equation, which considers a finite diffusion layer thickness with absorbing boundary condition:

$$Z_{ws} = \frac{R_w \tanh(B\sqrt{j\omega})}{B\sqrt{j\omega}} \quad (4)$$

where  $B = \delta/(D)^{1/2}$ ,  $D$  is the diffusion coefficient of the diffusing particles,  $\delta$  is the diffusion layer thickness and  $R_w$  is the Warburg resistance.

The values of the different parameters of the equivalent circuit in (**Figure 8**) are shown in **Table 6**.  $C_I$  values have been calculated from the CPE impedance using equation (2).

The values of  $\chi^2$  are of the order of  $10^{-3}$ , indicating that the fittings are good from a mathematical point of view.

It can be observed from **Table 6** that the charge transfer resistance,  $R_I$ , is higher in the non-polluted seawater for the Alloy 900, which reflects the better protective properties of the passive film formed in this electrolyte. Therefore, charge transfer processes at the passive film/electrolyte interface are enhanced in the polluted seawater.

On the other hand, the capacitance of the passive film/electrolyte interface,  $C_I$ , increases in the polluted electrolyte. The interfacial capacitance has a strong influence on electrochemical processes in passive systems, since its characteristics determine the potential drop at the semiconducting passive film/electrolyte interface [15, 38, 39]. Therefore, an increase in  $C_I$  for the passive film formed in the polluted seawater suggests, along with the decrease observed in  $R_I$ , worse protective properties of this passive film against corrosion. The high values of the exponent  $n_I$  (equal to or higher than 0.90 in all the cases) reveal that CPEs correspond to a nearly capacitive response, and support the introduction of CPEs in the equivalent circuit rather than pure capacitors.

The Warburg resistance,  $R_W$ , also decreases for passive films formed in the polluted seawater, indicating an enhancement of point defects transport through the passive film which, in turn, results in higher passive current densities as it has been observed in **Table 3**. The last parameter presented in **Table 6** is the Warburg coefficient,  $\sigma$ , calculated using the next relationship:

$$\sigma = \frac{R_W}{B \times \sqrt{2}} \quad (5)$$

The Warburg coefficient is inversely proportional to the concentration of diffusing species, which in the present case are the point defects within the passive film [30, 40].  $\sigma$  values are always lower in the polluted seawater, indicating an increase in the concentration of point defects in the passive films formed in this medium.

Concerning the comparison between the protective properties of passive films formed on both stainless steels,  $R_I$  values are more than 10 times higher and  $C_I$  is always lower in the case of Alloy 900, regardless of the type of seawater (**Table 6**). Besides,  $R_W$  and  $\sigma$  values are appreciably higher for Alloy 900, indicating that the number of defects within the passive film is lower in the case of Alloy 900, and that the transport of these defects through the film is slower for Alloy 900 than for AISI 316 SS. All these results denote a better resistance against corrosion of passive films formed on Alloy 900 if compared with those formed on AISI 316 SS.

### 3.6. Mott-Schottky analysis

To study the influence of the different seawaters on the semiconducting properties of passive films formed on AISI 316 SS and Alloy 900, the Mott-Schottky (MS) analysis has been performed. **Figure 9** shows the variation of  $C^{-2}$  vs.  $E$  at a constant frequency of 5000 Hz. In a previous work [7], it was observed that the capacitance-potential curves obtained for a stainless steel in seawater were strongly dependent on frequency at frequencies lower than 5000 Hz. At 5000 Hz, however, the capacitance became almost independent on frequency. Consequently, a value of 5000 Hz has been used in the

present work to perform MS analysis, thus avoiding the capacitance dependence on frequency.

The measured capacitance of the passive system can be written as:

$$\frac{1}{C} = \frac{1}{C_{SC}} + \frac{1}{C_H} \quad (6)$$

where  $C_{SC}$  is the capacitance of the space charge layer and  $C_H$  the capacitance of the Helmholtz layer.

From eq. (6), the Mott-Schottky relations for  $p$ -type and  $n$ -type semiconductors are expressed by eqs. (7) and (8) respectively:

$$\frac{1}{C^2} = \frac{1}{C_H^2} - \frac{2}{\epsilon\epsilon_0 e N_A} \left( E - E_{FB} - \frac{kT}{e} \right) \quad \mathbf{p\text{-type}} \quad (7)$$

$$\frac{1}{C^2} = \frac{1}{C_H^2} + \frac{2}{\epsilon\epsilon_0 e N_D} \left( E - E_{FB} - \frac{kT}{e} \right) \quad \mathbf{n\text{-type}} \quad (8)$$

where  $\epsilon$  is the dielectric constant of the passive film (a value of 15.6 has been assumed for the chromium and iron oxides formed on austenitic stainless steels <sup>[41]</sup>),  $\epsilon_0$  is the vacuum permittivity ( $8.85 \cdot 10^{-14}$  F/cm),  $e$  is the electron charge ( $1.602 \cdot 10^{-19}$  C),  $N_A$  and  $N_D$  are respectively the acceptor and donor densities,  $E_{FB}$  is the flat-band potential,  $k$  is the Boltzmann constant ( $1.38 \cdot 10^{-23}$  J/K) and  $T$  is the absolute temperature.

Two linear regions can be observed in the MS plots shown in **Figure 9** for the passive films formed on both stainless steels in both seawater media. One of these linear regions has a positive slope (at high potential values), while the other linear region displays a negative slope (at lower potentials). The presence of a straight line with a negative slope in MS diagrams is characteristic of *p*-type semiconductors, whereas the straight line with a positive slope is characteristic of *n*-type semiconductors. It is normally assumed that the semiconducting behaviour of stainless steels reveals a duplex structure of their passive films [8, 15, 20, 42-46]. The inner region of the passive film is made up a mixed oxide Fe-Cr or Fe-Cr-Ni with a spinel structure which may display both *p*-type or *n*-type semiconducting behaviour, depending on the relative amount of Cr(III) or Fe(III) [46, 47]. The outer region of the passive film consists of a layer of precipitated iron and chromium hydroxides and oxy-hydroxides, which behave as an *n*-type semiconductor [46-48].

A clear influence of the type of seawater on the slope and the capacitance values of the linear region at high potentials can be observed for both stainless steels (**Figure 9**). This linear region at high potentials has been related above to the part of the inner layer of the passive which displays *n*-type semiconductivity and to the outer layer of the passive film (which behaves as an *n*-type semiconductor, as well). On the other hand, the influence of the type of seawater on the linear region at very negative potentials is less marked. The negative slope remains approximately constant, regardless of the seawater used, while the capacitance values tend to decrease slightly in the polluted seawater, indicating a thicker space charge layer in the innermost region of the film. This linear region with a negative slope that appears at the most negative potentials is associated with the semiconducting behaviour of the innermost layer of the passive film (*p*-type

semiconductor). In the case of the  $p$ -type space charge layer, only its thickness is modified in the polluted seawater, whereas the density of defects (inversely proportional to the value of the negative slope, according to eq. (7)) remains approximately constant. Therefore, the nature of the seawater affects specially the defect structure and the thickness of the space charge layer developed in the  $n$ -type semiconductivity region.

The density of defects within the different space charge regions developed in the AISI 316 SS and Alloy 900 passive films (acceptor,  $N_A$ , and donors,  $N_D$ ) can be determined from the slopes of the linear zones observed in the MS diagrams (**Figure 9**) using the equations (7) and (8), respectively. In  $p$ -type space charge regions, the predominant acceptor species are cation vacancies ( $V_{Cr}^{3\cdot}$  in this case), while in  $n$ -type space charge regions oxygen vacancies ( $V_O^{\cdot\cdot}$ ) and cation interstitials ( $Cr_i^{3+}$  in this case) are the main donor species. Kroger-Vink notation is used for the effective positive ( $\cdot\cdot$ ) and negative ( $^{3\cdot}$ ) charges in oxygen and cation vacancies, respectively. The values of  $N_A$  and  $N_D$  for both stainless steels in non-polluted and polluted seawater at 25° C are shown in **Table 7**.

It can be observed from **Table 7** that the density of oxygen vacancies and/or cation interstitials, which are predominant in the  $n$ -type space charge region,  $N_D$ , increases more than two times for the stainless steels passivated in the polluted seawater, comparing with the samples passivated in the non-polluted seawater. This result indicates that the part of the inner layer of the film with an  $n$ -type semiconducting behavior, as well as the outer layer of the film, have a more disordered structure in the polluted seawater, with a higher concentration of defects.

The higher values of  $N_D$  in the polluted seawater are a consequence of the lower pH of this electrolyte, since an increase in  $H^+$  concentration (acceptor species<sup>[49]</sup>) will enhance the reaction of  $H^+$  with the oxygen present in the passive film, leading to an increase in the amount of oxygen vacancies. Concerning the density of defects existing in the innermost layer of the passive film ( $N_A$ , with  $p$ -type semiconducting behavior), no clear tendency is observed in **Table 7**, so the type of seawater does not have an evident influence on the defectiveness of this innermost layer.

Comparing both stainless steels, it can be observed from **Table 7** that passive films formed on Alloy 900 have slightly lower densities of donor species ( $N_D$ ), regardless of the used electrolyte. This decrease in  $N_D$  may be related to the higher Cr content present in Alloy 900, since a higher amount of Cr in the composition of the passive film could result in a lower concentration of cation interstitials ( $Cr_i^{3+}$ ) in the  $n$ -type semiconductivity region of the passive film.

The thickness of the space charge layers formed within the passive film ( $d_{SC}$ ) can be estimated from the  $C_{SC}$  values determined at the formation potential (thickness of the  $n$ -type space charge layer) and at the most negative potential (thickness of the  $p$ -type space charge layer). Thicknesses have been calculated with the expression for a parallel plane condenser given in eq. (3)<sup>[43]</sup>:

The values of  $C_{SC}$  necessary to estimate  $d_{SC}$  have been determined from the total measured capacitance ( $C$ ) and the Helmholtz layer capacitance ( $C_H$ ) using eq. (6). To obtain the values of  $C_H$ , it has been assumed that the minimum point in the  $C^{-2}$  vs  $E$  plot (at the flat band potential,  $E = E_{FB}$ ),  $C_H$  is equal to the total measured capacitance, since

no depletion layer exists at this potential and the contribution of the space charge or the passive film to the total capacitance values is negligible<sup>[50, 51]</sup>. From **Figure 9**  $C_H$  values were estimated to be  $28.6 \mu\text{F cm}^{-2}$  and  $28.0 \mu\text{F cm}^{-2}$  (AISI 316 SS in non-polluted and polluted seawater, respectively), and  $28.3 \mu\text{F cm}^{-2}$  and  $21.8 \mu\text{F cm}^{-2}$  (Alloy 900 in non-polluted and polluted seawater, respectively).

The thicknesses of the  $p$ -type space charge layer ( $d_{SC_p}$ ) and the  $n$ -type space charge layer ( $d_{SC_n}$ ) formed within the passive films of AISI 316 SS and Alloy 900 in both non-polluted and polluted seawaters are shown in **Table 8**. It can be observed that the thickness of the  $n$ -type space charge region ( $d_{SC_n}$ ) decreases considerably in the polluted seawater, regardless of the used stainless steel, while the thickness of the  $p$ -type space charge region ( $d_{SC_p}$ ) increases in the case of AISI 316 SS and remains approximately constant for Alloy 900. The lower pH value observed in the polluted seawater results in a higher dissolution rate of the iron species that make up the outer passive film layer, thus decreasing the total thickness of the  $n$ -type space charge layer<sup>[6]</sup>. On the other hand, the increase in  $d_{SC_p}$  observed for AISI 316 SS in the polluted seawater can also be explained by the lower pH value of this electrolyte, since it has been observed<sup>[6]</sup> that a decrease in pH leads to an enrichment in chromium within the passive films formed on AISI 316 SS, resulting in a higher thickness of the innermost layer of the film. However, this increase in  $d_{SC_p}$  in the polluted seawater is not accompanied by an improvement of the protective properties of the passive films formed in that electrolyte, since it has been confirmed above (**Table 6**) that the resistance of these films decrease in the polluted seawater as a consequence of a more defective structure (**Table 7**).

#### 4. Conclusions

EIS measurements at open circuit potential demonstrate that the protection provided by the passive films formed on the different alloys was mainly due to the inner oxide film. Lower values on the polarisation resistance were obtained for both steels in the polluted seawater, indicating a slightly higher electrical conductivity on these passive films. These results are in concordance with the behaviour observed in the potentiodynamic curves.

The current-time transients showed that the passivation process taking place in the polluted seawater was slowed down for both alloys. Hence, the composition of the polluted seawater negatively affects the passivation kinetics of both AISI 316SS and Alloy 900.

Passive films formed in the polluted seawater presented lower resistance values and a more defective structure in the *n*-type semiconducting region than those formed in unpolluted seawater, for the two studied stainless steels (AISI 316 SS and Alloy 900).

The thickness of the *n*-type space charge region ( $d_{SC_n}$ ) has been observed to decrease considerably in the polluted seawater, regardless of the used stainless steel, while the thickness of the *p*-type space charge region ( $d_{SC_p}$ ) increased in the case of AISI 316 SS and remained approximately constant for Alloy 900. Both results have been explained taking into account the lower pH value in the polluted electrolyte.

Comparing both stainless steels, it can be concluded that passive films formed on Alloy 900 presented significantly better protective properties than those on AISI 316 SS, showing higher values of  $R_L$ ,  $R_W$  and  $\sigma$ , and lower values of  $C_L$ , regardless of the used seawater. Moreover,  $N_D$  was lower in the case of Alloy 900, which supports the previous results and the results observed in the potentiodynamic curves.

## ACKNOWLEDGEMENTS

We wish to express our gratitude to Prof. Dr. Aurora Santos López, Dr. Rosario Lunar Hernández and Dr. Jose Arnosó Sampedro (Instituto de Geociencias (CSIC, UCM)), Dr. Carmen López Moreno (Head of the Volcano Monitoring Unit, Spanish National Geographic Institute), Humberto Gutiérrez García (Head of the Civil Protection and Emergency Management Service of the General Directorate of Security and Emergencies of the Canary Islands) and Alejandro Ramos Fernández (Coordinador Multisectorial del Centro Coordinador de Emergencias 112 del Gobierno de Canarias) for their help in supplying both non-polluted and polluted seawater samples and to Dr. M. Asunción Jaime for her translation assistance.

## References

- [1] G. Chiodini, S. Caliro, G. Caramanna, D. Granieri, C. Minopoli, R. Moretti, L. Perotta, G. Ventura. *Geochemistry of the Submarine Gaseous Emissions of Panarea (Aeolian Islands, Southern Italy): Magmatic vs. Hydrothermal Origin and Implications for Volcanic Surveillance*, Pure Appl. Geophys. 163 (2006) 759-780.
- [2] A. Esposito, G. Giordano, M. Anzidei. *The 2002-2003 submarine gas eruption at Panarea volcano (Aeolian Islands, Italy): Volcanology of the seafloor and implications for the hazard scenario*, Mar. Geol. 227 (2006) 119-134.
- [3] P. Sedwick, D. Stuben. *Chemistry of shallow submarine warm springs in an arc-volcanic setting: Vulcano Island, Aeolian Archipelago, Italy*, Mar. Chem. 53 (1996) 147-161.
- [4] C. Siebe, J. C. Komorowski, C. Navarro, J. McHone, H. Delgado, A. Cortés. *Submarine eruption near Socorro Island, Mexico: Geochemistry and scanning electron microscopy studies of floating scoria and reticulite*, J. Volcanol. Geoth. Res. 68 (1995) 239-271.

- [5] J. Duan, S. Wu, X. Zhang, G. Huang, M. Du, B. Hou. *Corrosion of carbon steel influenced by anaerobic biofilm in natural seawater*, *Electrochim. Acta* 54 (2008) 22-28.
- [6] L. Freire, M. J. Carmezim, M. G. S. Ferreira, M. F. Montemor. *The passive behaviour of AISI 316 in alkaline media and the effect of pH: A combined electrochemical and analytical study*, *Electrochim. Acta* 55 (2010) 6174-6181.
- [7] R.M. Fernández-Domene, R. Sánchez-Tovar, C. Escrivà-Cerdán, R. Leiva-García, J. García-Antón. *Study of Passive Films Formed on AISI 316L Stainless Steel in Non-Polluted and Underwater-Volcano-Polluted Seawater*. *Corrosion* 70, (2014) 390-401.
- [8] N. E. Hakiki, S. Boudin, B. Rondot, M. Da Cunha Belo. *The electronic structure of passive films formed on stainless steels*, *Corros. Sci.* 37 (1995) 1809-1822.
- [9] R. C. Newman. 2001 W.R. Whitney Award Lecture: *Understanding the Corrosion of Stainless Steel*, *Corrosion* 57 (2001) 1030-1041.
- [10] M. Kaneko, H. S. Isaacs. *Pitting of stainless steel in bromide, chloride and bromide/chloride solutions*, *Corros. Sci.* 42 (2000) 67-78.
- [11] M. Kaneko, H. S. Isaacs. *Effects of molybdenum on the pitting of ferritic- and austenitic-stainless steels in bromide and chloride solutions*, *Corros. Sci.* 44 (2002) 1825-1834.
- [12] J. Pan, D. Thierry, C. Leygraf. *Electrochemical impedance spectroscopy study of the passive oxide film on titanium for implant application*, *Electrochim. Acta* 41 (1996) 1143-1153.
- [13] S. L. d. Assis, S. Wolyneć, I. Costa. *Corrosion characterization of titanium alloys by electrochemical techniques*, *Electrochim. Acta* 51 (2006) 1815-1819.
- [14] A. Igual-Muñoz, J. García-Antón, J. L. Guiñón, V. Pérez-Herranz. *Inhibition effect of chromate on the passivation and pitting corrosion of a duplex stainless steel in LiBr solutions using electrochemical techniques*, *Corrosion Science* 49 (2007) 3200-3225.
- [15] R. M. Fernández-Domene, E. Blasco-Tamarit, D. M. García-García, J. García-Antón. *Passive and Transpassive Behaviour of Alloy 31 in a Heavy Brine LiBr Solution*, *Electrochim. Acta* 95 (2013) 1-11.
- [16] G.J. Brug, A.L.G. Vandeneeden, M. Sluytersrehabach, J.H. Sluyters, *The analysis of electrode impedances complicated by the presence of a constant phase element*, *Journal of Electroanalytical Chemistry* 176 (1984) 275-295.
- [17] B. Evgenij, J. Ros Macdonald, *Impedance Spectroscopy: Theory, Experiment and Applications*, 2nd ed., West Sussex, UK, 2005.
- [18] J. Pan, C. Leygraf, R.F.A. Jargelius-Pettersson, J. Linden, *Characterization of High-Temperature Oxide Films on Stainless Steels by Electrochemical-Impedance Spectroscopy*, *Oxidation of Metals* 50 (1998) 431-455.
- [19] M. F. Montemor, M. G. S. Ferreira, N. E. Hakiki, M. Cunha Belo, *Chemical composition and electronic structure of the oxide films formed on 316L stainless steel and nickel based alloys in high temperature aqueous environments*, *Corrosion Science* 42 (2000) 1635-1650.
- [20] M. G. S. Ferreira, N. E. Hakiki, G. Goodlet, S. Faty, A. M. P. Simoes, M. Da Cunha Belo. *Influence of the temperature of film formation on the electronic structure of oxide films formed on 304 stainless steel*, *Electrochimica Acta* 46 (2001) 3767-3776.
- [21] C. Escrivà-Cerdán, E. Blasco-Tamarit, D.M. García-García, J. García-Antón, A. Guenbour, *Effect of potential formation on the electrochemical behaviour of a*

- highly alloyed austenitic stainless steel in contaminated phosphoric acid at different temperatures*, *Electrochimica Acta* 80 (2012) 248-256.
- [22] S. Yagi, A. Sengoku, K. Kubota, E. Matsubara, *Surface modification of ACM522 magnesium alloy by plasma electrolytic oxidation in phosphate electrolyte*, *Corrosion Science* 57 (2012) 74-80.
- [23] D.D. Macdonald, A. Sun, N. Priyantha, P. Jayaweera, *An electrochemical impedance study of Alloy-22 in NaCl brine at elevated temperature: II. Reaction mechanism analysis*, *Journal of Electroanalytical Chemistry* 572 (2004) 421-431.
- [24] R.M. Fernández-Domene, E. Blasco-Tamarit, D.M. García-García, J. García-Antón, *Cavitation corrosion and repassivation kinetics of titanium in a heavy brine LiBr solution evaluated by using electrochemical techniques and Confocal Laser Scanning Microscopy*, *Electrochimica Acta* 58 (2011) 264-275.
- [25] C. Escrivà-Cerdán, E. Blasco-Tamarit, D.M. García-García, J. García-Antón, A. Guenbour, *Passivation behaviour of Alloy 31 (UNS N08031) in polluted phosphoric acid at different temperatures*, *Corrosion Science* 56 (2012) 114-122.
- [26] H.S. Kwon, E.A. Cho, K.A. Yeom, *Prediction of Stress Corrosion Cracking Susceptibility of Stainless Steels Based on Repassivation Kinetics*, *Corrosion* 56 (2000) 32-40.
- [27] R.M. Carranza, J.R. Galvele, *Repassivation kinetics in stress corrosion cracking—I. Type AISI 304 stainless steel in chloride solutions*, *Corrosion Science* 28 (1988) 233-249.
- [28] F.M. Song, K.S. Raja, D.A. Jones, *A film repassivation kinetic model for potential-controlled slower electrode straining*, *Corrosion Science* 48 (2006) 285-307.
- [29] S. Ahila, B. Reynders, H. J. Grabke, *The evaluation of the repassivation tendency of Cr-Mn and Cr-Ni steels using scratch technique*, *Corrosion Science* 38 (1996) 1991-2005.
- [30] M. Sánchez, J. Gregori, M. C. Alonso, J. J. García-Jareño, F. Vicente. *Anodic growth of passive layers on steel rebars in an alkaline medium simulating the concrete pores*, *Electrochimica Acta* 52 (2006) 47-53.
- [31] M. Sánchez, J. Gregori, C. Alonso, J. J. García-Jareño, H. Takenouti, F. Vicente. *Electrochemical impedance spectroscopy for studying passive layers on steel rebars immersed in alkaline solutions simulating concrete pores*, *Electrochimica Acta* 52 (2007) 7634-7641.
- [32] C. Y. Chao, L. F. Lin, D. D. Macdonald. *A Point Defect Model for Anodic Passive Films III. Impedance Response*, *J. Electrochem. Soc.* 129 (1982) 1874-1879.
- [33] D. D. Macdonald, R. Y. Liang, B. G. Pound. *An Electrochemical Impedance Study of the Passive Film on Single Crystal Ni(111) in Phosphate Solutions*, *Journal of the Electrochemical Society* 134 (1987) 2981-2986.
- [34] M. G. S. Ferreira, J. L. Dawson. *Electrochemical Studies of the Passive Film on 316 Stainless Steel in Chloride Media*, *J. Electrochem. Soc.* 132 (1985) 760-765.
- [35] C. Boissy, C. Alemany-Dumont, B. Normand. *EIS evaluation of steady-state characteristic of 316L stainless steel passive film grown in acidic solution*, *Electrochemistry Communications* 26 (2013) 10-12.
- [36] Z. Grubac, Z. Petrovic, J. Katic, M. Metikos-Hukovic, R. Babic. *The electrochemical behaviour of nanocrystalline nickel: A comparison with*

- polycrystalline nickel under the same experimental condition*, Journal of Electroanalytical Chemistry 645 (2010) 87-93.
- [37] H. Zhang, Y. L. Zhao, Z. D. Jiang. *Effects of temperature on the corrosion behavior of <sup>13</sup>Cr martensitic stainless steel during exposure to CO<sub>2</sub> and Cl<sup>-</sup> environment*, Materials Letters 59 (2005) 3370-3374.
- [38] J. O. Bockris. *Interfacial electron transfer as a significant step in photoelectrochemical reactions on some semiconductors*, J. Appl. Phys. 52 (1981) 808-810.
- [39] K. Uosaki, H. Kita. *Effects of the Helmholtz Layer Capacitance on the Potential Distribution at Semiconductor/Electrolyte Interface and the Linearity of the Mott-Schottky Plot*, J. Electrochem. Soc. 130 (1983) 895-897.
- [40] Z. Grubac, M. Metikos-Hukovic. *EIS study of solid-state transformations in the passivation process of bismuth in sulfide solution*, Journal of Electroanalytical Chemistry 565 (2004) 85-94.
- [41] A. D. Paola. *Semiconducting properties of passive films on stainless steels*, Electrochim. Acta 34 (1989) 203-210.
- [42] N. E. Hakiki, M. Da Cunha Belo, A. M. P. Simoes, M. G. S. Ferreira. *Semiconducting Properties of Passive Films Formed on Stainless Steels*, Journal of the Electrochemical Society 145 (1998) 3821-3829.
- [43] M. Da Cunha Belo, N. E. Hakiki, M. G. S. Ferreira. *Semiconducting properties of passive films formed on nickel-base alloys type Alloy 600: influence of the alloying elements*, Electrochim. Acta 44 (1999) 2473-2481.
- [44] G. Lothongkum, S. Chaikittisilp, A. W. Lothongkum. *XPS investigation of surface films on high Cr-Ni ferritic and austenitic stainless steels*, Applied Surface Science 218 (2003) 203-210.
- [45] C.-O. A. Olsson, D. Landolt. *Passive films on stainless steels--chemistry, structure and growth*, Electrochim. Acta 48 (2003) 1093-1104.
- [46] T. L. S. Wijesinghe, D. J. Blackwood. *Characterisation of passive films on 300 series stainless steels*, Appl. Surf. Sci. 253 (2006) 1006-1009.
- [47] R.M. Fernández-Domene, E. Blasco-Tamarit, D.M. García-García, J. García-Antón, *Effect of alloying elements on the electronic properties of thin passive films formed on carbon steel, ferritic and austenitic stainless steels in a highly concentrated LiBr solution*, Thin Solid Films 558 (2014) 252-258.
- [48] T.L.S.L. Wijesinghe, D.J. Blackwood. *Electrochemical and Photoelectrochemical Characterization of the Passive Film Formed on AISI 254SMO Super-Austenitic Stainless Steel*, J. Electrochem. Soc. 154 (2007) C16-C23.
- [49] J. Amri, T. Souier, B. Malki, B. Baroux. *Effect of the final annealing of cold rolled stainless steels sheets on the electronic properties and pit nucleation resistance of passive films*, Corros. Sci. 50 (2008) 431-435.
- [50] W. P. Gomes, D. Vanmaekelbergh. *Impedance spectroscopy at semiconductor electrodes: Review and recent developments*, Electrochim. Acta 41 (1996) 967-973.
- [51] N. E. Hakiki, M. Da Cunha Belo. *Electronic Structure of Passive Films Formed on Molybdenum-Containing Ferritic Stainless Steels*, Journal of the Electrochemical Society 143 (1996) 3088-3093.

## Table Captions

**Table 1.** Chemical composition in weight % of AISI 316 and Alloy 900 stainless steels.

**Table 2.** Open circuit potential values for AISI 316 and Alloy 900 in both non-polluted and polluted seawater.

**Table 3.** Electrochemical parameters for AISI 316 and Alloy 900 in both non-polluted and polluted seawater, obtained from cyclic polarization curves.

**Table 4.** Equivalent circuit parameters obtained by fitting the experimental results of EIS, for AISI 316L and Alloy 900 in both non-polluted and polluted seawater, at the open circuit potential .

**Table 5.** Passivation times,  $t_p$  and steady-state current density,  $i_{ss}$  for AISI 316SS and Alloy 900 in both non-polluted and polluted seawater.

**Table 6.** Equivalent circuit parameters obtained by fitting the experimental results of EIS, for AISI 316L and Alloy 900 in both non-polluted and polluted seawater, at the  $-0.1 V_{Ag/AgCl}$ .

**Table 7.** Acceptor and donor densities ( $N_A$  and  $N_D$ , respectively) for AISI 316 and Alloy 900 in both non-polluted and polluted seawater, at the different film formation potentials within the passive range.

**Table 8.** Thicknesses of the inner ( $d_{SC_p}$ ) and outer ( $d_{SC_n}$ ) space charge layers for AISI 316 and Alloy 900 in both non-polluted and polluted seawater, at the different film formation potentials within the passive range.

## Figure Captions

**Figure 1.** Potentiodynamic polarization cyclic curves for AISI 316 and Alloy 900 in both non-polluted and polluted seawater solutions at 25° C.

**Figure 2.** Nyquist (a) and Bode-phase (b) plots for AISI 316 SS in both non-polluted and polluted seawater at 25° C, at Open circuit potential.

**Figure 3.** Nyquist (a) and Bode-phase (b) plots for Alloy 900 in both non-polluted and polluted seawater at 25° C, at Open Circuit Potential.

**Figure 4.** Representation of the equivalent circuit proposed for the interpretation of EIS spectra of AISI 316 and Alloy 900 in the seawater solutions under study, at Open circuit potential.

**Figure 5.** Current density transients for AISI 316SS (a) and Alloy 900 (b) recorded after stepping the potential from the cathodic cleaning value ( $-0.4 V_{Ag/AgCl}$ ) to the film formation potential ( $-0.1 V_{Ag/AgCl}$ ), in both non-polluted and polluted seawater at 25° C.

**Figure 6.** Nyquist (a) and Bode-phase (b) plots for AISI 316 SS in both non-polluted and polluted seawater at 25° C, at a film formation potential of  $-0.1 V_{Ag/AgCl}$ .

**Figure 7.** Nyquist (a) and Bode-phase (b) plots for Alloy 900 in both non-polluted and polluted seawater at 25° C, at a film formation potential of  $-0.1 V_{Ag/AgCl}$ .

**Figure 8.** Representation of the equivalent circuit proposed for the interpretation of EIS spectra of AISI 316 and Alloy 900 in the seawater solutions under study, at a film formation potential of  $-0.1 V_{Ag/AgCl}$ .

**Figure 9.** Capacitance-potential curves obtained at 5 KHz for AISI 316 (a) and Alloy 900 (b) in the polluted and non-polluted seawater at 25° C, scanning the potential from the film formation value of  $-0.1 V_{Ag/AgCl}$  in the negative direction.

	<b>Cr</b>	<b>Ni</b>	<b>Mn</b>	<b>Mo</b>	<b>S</b>	<b>Si</b>	<b>P</b>	<b>C</b>	<b>Fe</b>	<b>Cu</b>	<b>N</b>	<b>Ti</b>
<b>AISI 316</b>	16.96	10.17	1.34	2.30	0.00	0.37	0.03	0.02	Bal.	--	--	--
<b>Alloy 900</b>	22.34	4.85	1.59	2.69	--	0.35	0.02	0.03	67.80	0.13	0.20	0.01

<b>Seawater</b>	<b>AISI 316</b>	<b>Alloy 900</b>
<b>Non-polluted</b>	$-90 \pm 7$	$-161 \pm 2$
<b>Polluted</b>	$-116 \pm 4$	$-155 \pm 8$

	$E_{\text{corr}}$ vs (Ag/AgCl)/mV	$i_p/\mu\text{A cm}^{-2}$	$E_p$ vs (Ag/AgCl)/mV	$E_{rp}$ vs (Ag/AgCl)/mV	$E_p - E_{rp}$ /mV
<b>Seawater</b>	<b>AISI 316</b>				
<b>Non-polluted</b>	$-230 \pm 8$	$3.89 \pm 0.32$	$309 \pm 10$	$-69 \pm 11$	378
<b>Polluted</b>	$-239 \pm 5$	$4.66 \pm 0.11$	$302 \pm 7$	$-55 \pm 15$	357
	<b>Alloy 900</b>				
<b>Non-polluted</b>	$-203 \pm 11$	$4.35 \pm 0.44$	$1220 \pm 47$	$990 \pm 22$	230
<b>Polluted</b>	$-197 \pm 6$	$5.02 \pm 0.09$	$1200 \pm 29$	$990 \pm 30$	210

		$R_s/\Omega \text{ cm}^2$	$R_1/k\Omega \text{ cm}^2$	$C_1/\mu\text{F cm}^{-2}$	$n_1$	$R_2/k\Omega \text{ cm}^2$	$C_2/\mu\text{F cm}^{-2}$	$n_2$	$R_p/k\Omega \text{ cm}^2$	$\chi^2 (\times 10^{-3})$
<b>AISI 316 SS</b>	<b>Non-polluted seawater</b>	$5.6 \pm 0.1$	$29 \pm 4$	$41.0 \pm 1.2$	$0.90 \pm 0.01$	$268 \pm 42$	$56.6 \pm 1.6$	$0.54 \pm 0.01$	297	4.4
	<b>Polluted seawater</b>	$5.8 \pm 0.2$	$52 \pm 8$	$68.4 \pm 1.9$	$0.92 \pm 0.01$	$152 \pm 32$	$105.0 \pm 2.1$	$0.64 \pm 0.01$	204	4.4
<b>Alloy 900</b>	<b>Non-polluted seawater</b>	$4.7 \pm 0.1$	$67 \pm 3$	$51.1 \pm 0.9$	$0.88 \pm 0.01$	$213 \pm 38$	$30.9 \pm 1.0$	$0.81 \pm 0.01$	280	4.8
	<b>Polluted seawater</b>	$4.7 \pm 0.1$	$49 \pm 5$	$68.2 \pm 1.1$	$0.91 \pm 0.01$	$180 \pm 34$	$26.6 \pm 1.2$	$0.82 \pm 0.01$	229	8.6

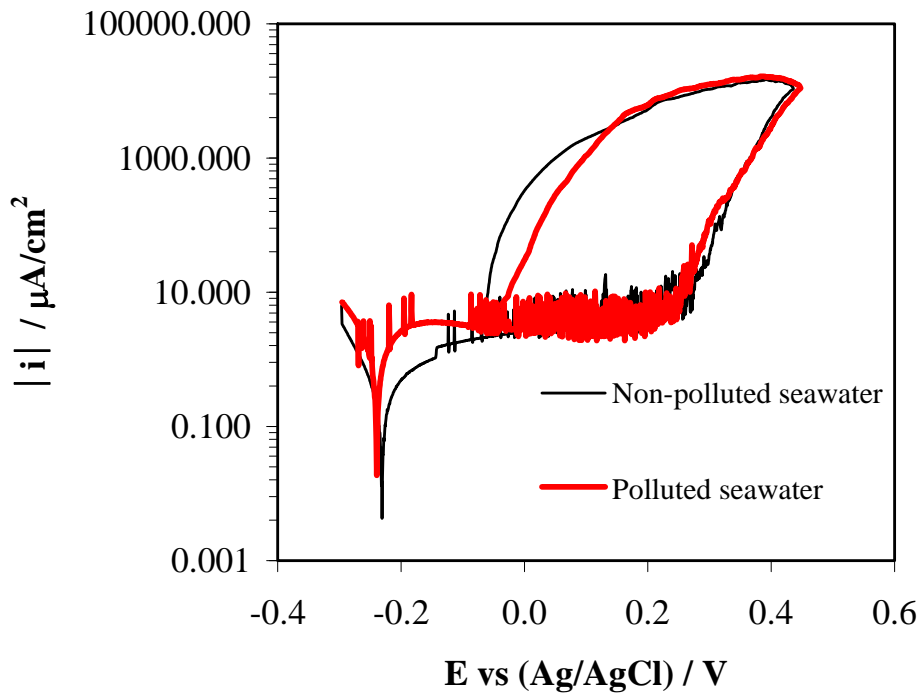
		$t_p$ (s)	$i_{ss}$ ( $\mu\text{A}/\text{cm}^2$ )
<b>AISI 316</b>	<b>Non-polluted seawater</b>	156	0.012
	<b>Polluted seawater</b>	505	0.014
<b>Alloy 900</b>	<b>Non-polluted seawater</b>	394	0.12
	<b>Polluted seawater</b>	668	0.14

		$R_s/\Omega \text{ cm}^2$	$R_f/k\Omega \text{ cm}^2$	$C_f/\mu\text{F cm}^{-2}$	$n_f$	$R_W/k\Omega \text{ cm}^2$	$\sigma/k\Omega \text{ cm}^2 \text{ s}^{-1/2}$	$\chi^2 (\times 10^{-3})$
<b>AISI 316 SS</b>	<b>Non-polluted seawater</b>	$5.4 \pm 0.1$	$26 \pm 4$	$16.2 \pm 1.1$	$0.90 \pm 0.01$	$295 \pm 14$	$50 \pm 3$	3.8
	<b>Polluted seawater</b>	$4.8 \pm 0.2$	$26 \pm 3$	$24.8 \pm 1.7$	$0.90 \pm 0.01$	$207 \pm 18$	$39 \pm 1$	3.7
<b>Alloy 900</b>	<b>Non-polluted seawater</b>	$4.7 \pm 0.3$	$535 \pm 30$	$12.4 \pm 1.3$	$0.91 \pm 0.01$	$753 \pm 53$	$118 \pm 10$	3.0
	<b>Polluted seawater</b>	$4.9 \pm 0.3$	$320 \pm 11$	$18.3 \pm 1.2$	$0.92 \pm 0.01$	$544 \pm 18$	$76 \pm 6$	2.7

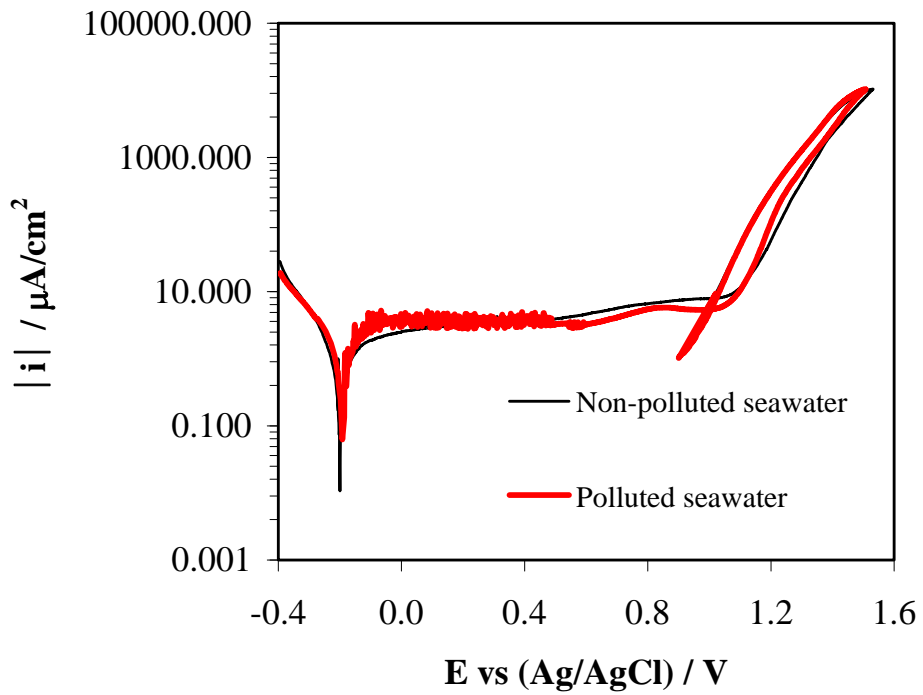
		$N_A/10^{20} \text{ cm}^{-3}$	$N_D/10^{20} \text{ cm}^{-3}$
<b>AISI 316 SS</b>	<b>Non-polluted seawater</b>	$10.4 \pm 0.3$	$4.7 \pm 0.02$
	<b>Polluted seawater</b>	$8.9 \pm 0.3$	$12.3 \pm 0.6$
<b>Alloy 900</b>	<b>Non-polluted seawater</b>	$8.6 \pm 1.2$	$4.0 \pm 0.8$
	<b>Polluted seawater</b>	$10.9 \pm 0.5$	$9.6 \pm 0.3$

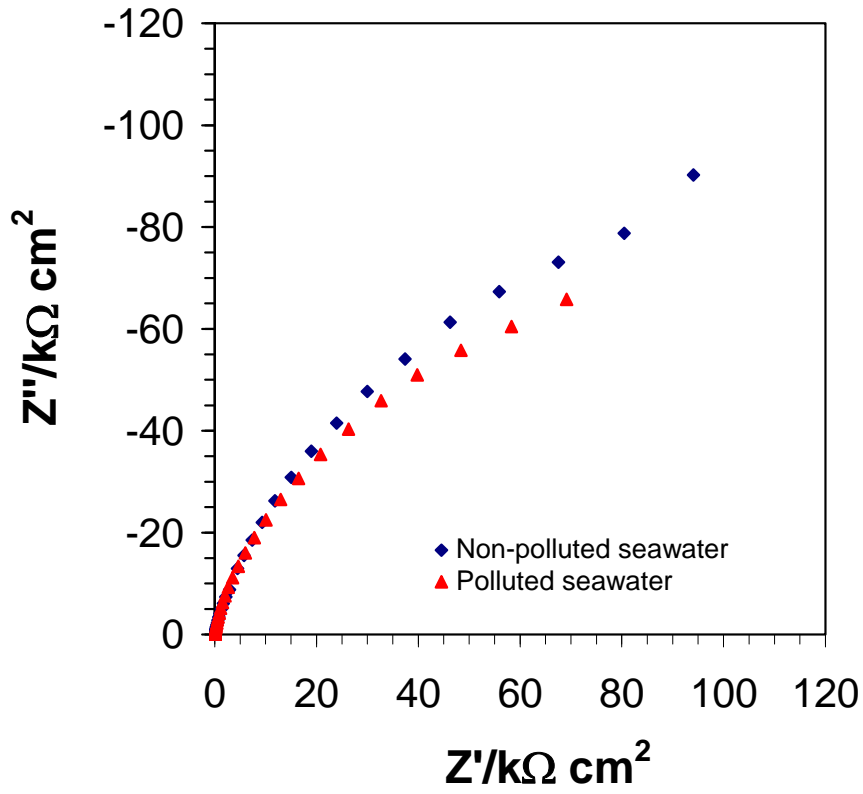
		$d_{SC_p} / \text{nm}$	$d_{SC_n} / \text{nm}$
<b>AISI 316 SS</b>	<b>Non-polluted seawater</b>	$0.37 \pm 0.02$	$0.54 \pm 0.02$
	<b>Polluted seawater</b>	$0.51 \pm 0.01$	$0.24 \pm 0.01$
<b>Alloy 900</b>	<b>Non-polluted seawater</b>	$0.51 \pm 0.02$	$0.57 \pm 0.01$
	<b>Polluted seawater</b>	$0.48 \pm 0.01$	$0.23 \pm 0.01$

a) AISI 316

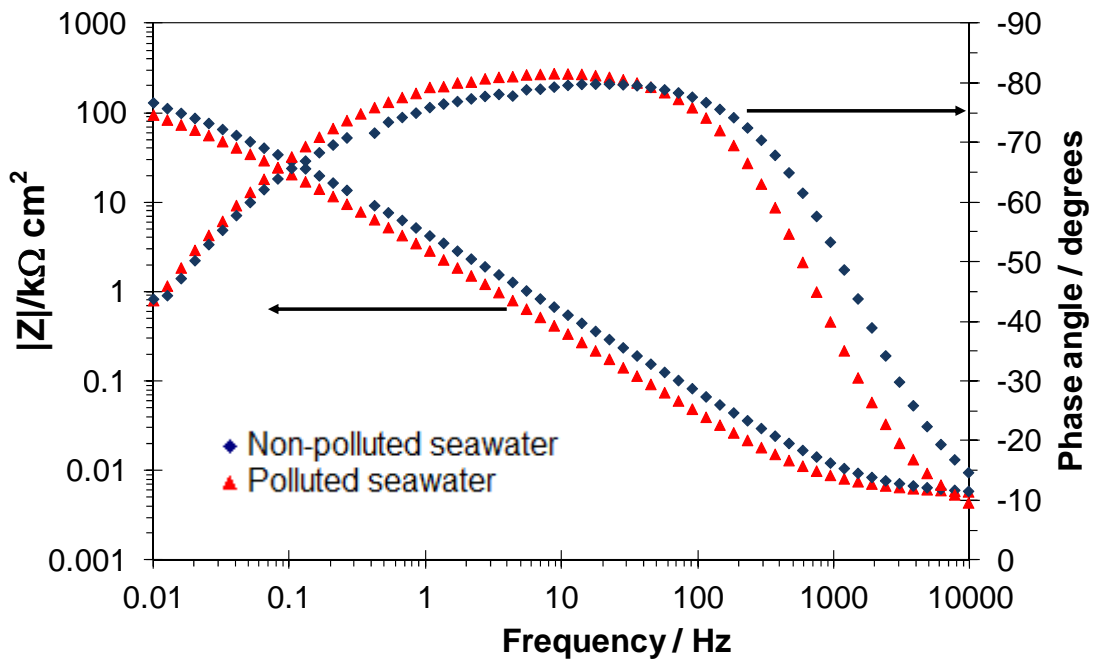


b) Alloy 900

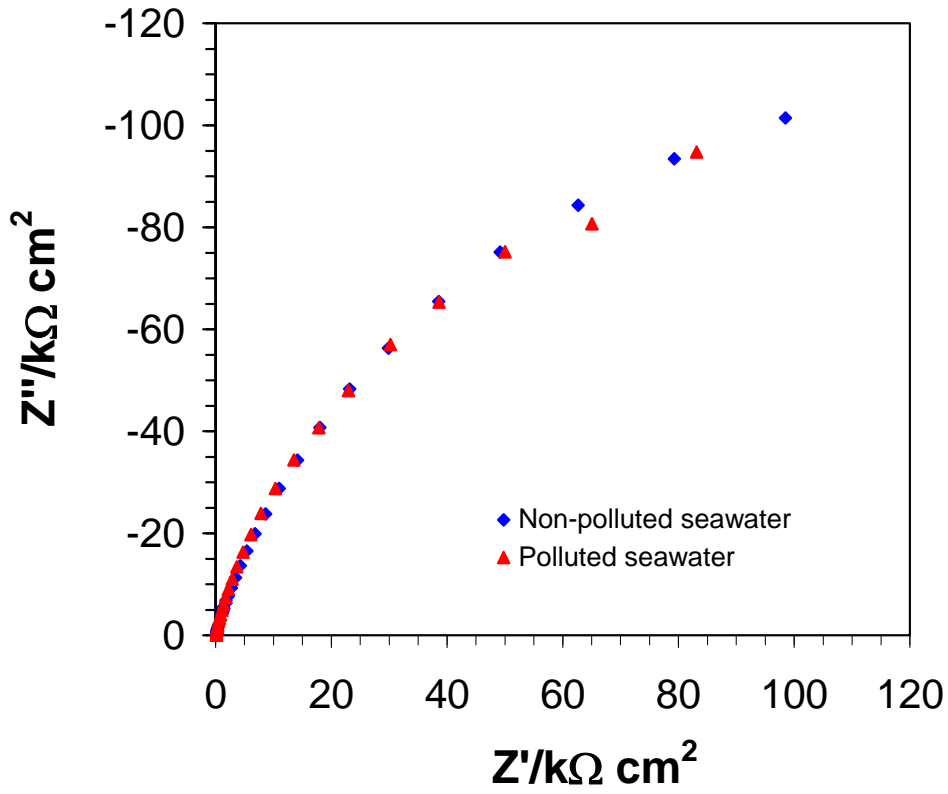




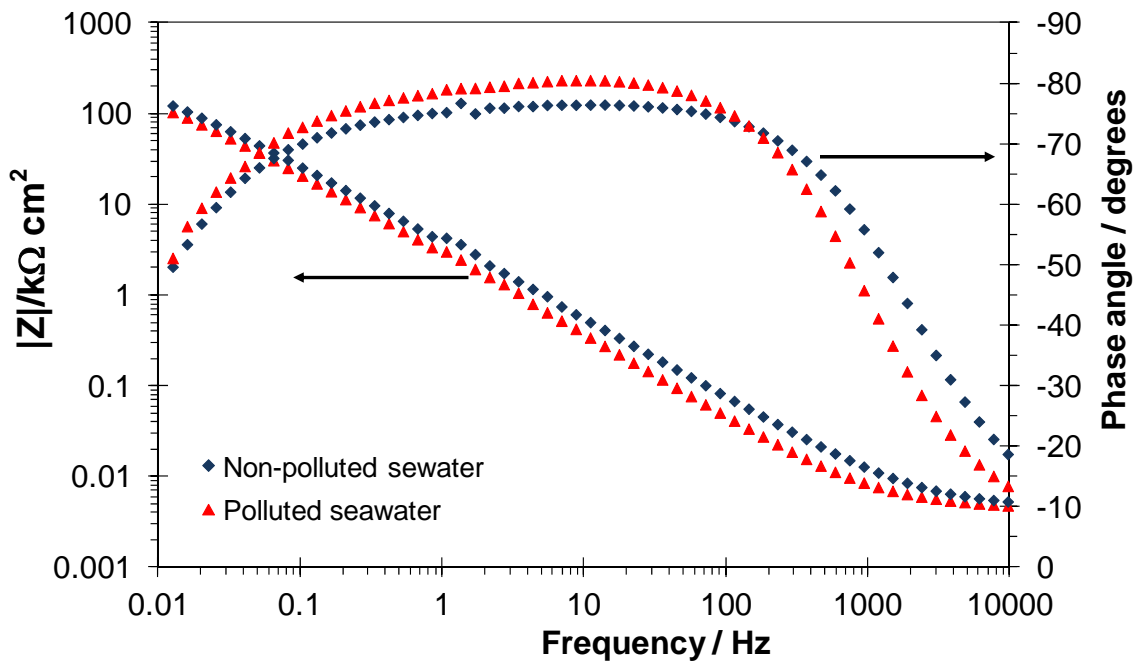
(a)



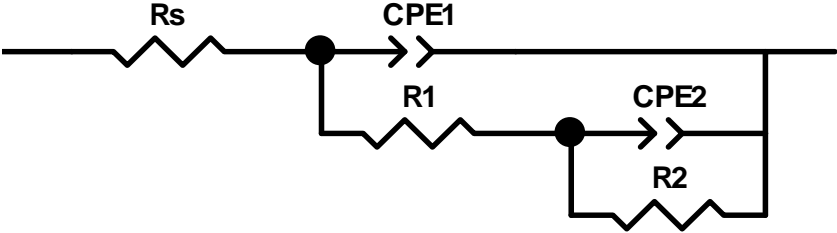
(b)

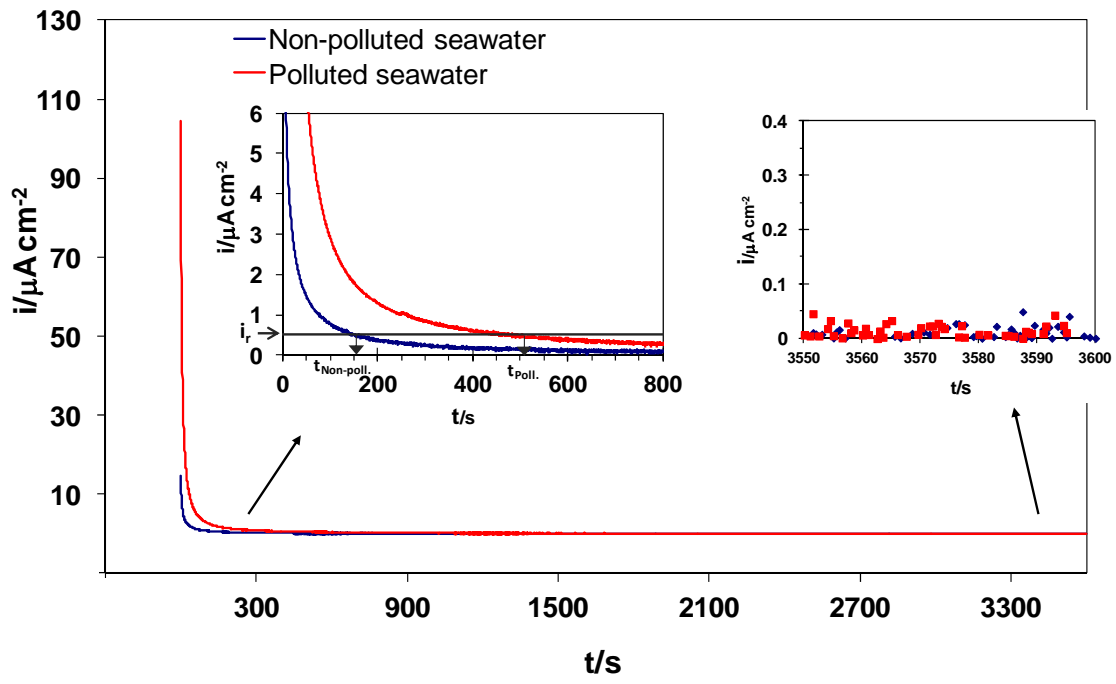


(a)

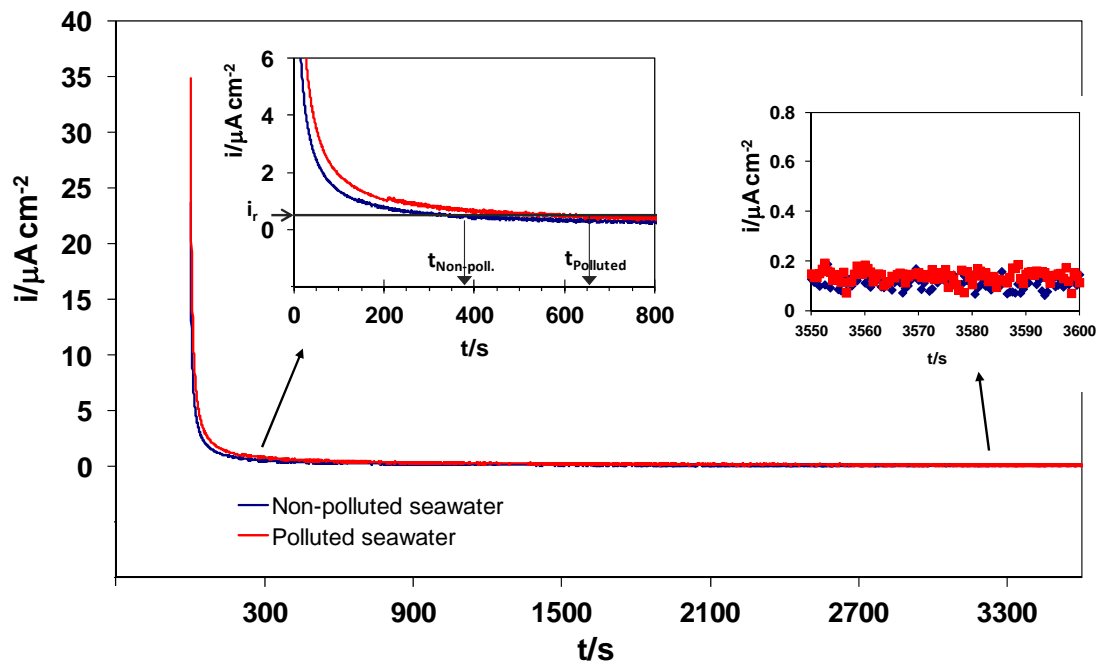


(b)





(a)



(b)

